Int. J. Electron. Commun. (AEÜ) 203 (2026) 156082

Contents lists available at ScienceDirect

International Journal of Electronics and Communications

journal homepage: www.elsevier.com/locate/aeue

Regular paper

Temperature stability and compensation of AMR sensors in practical applications

Matas Tamulynas [a], Eidenis Kasperavičius [a], Vytautas Markevičius [a], Dangirutis Navikas [a], Mindaugas Žilys [a], Algimantas Valinevičius [a], Michal Frivaldsky [b], Roman Sotner [c], Jan Jerabek [c], Darius Andriukaitis [a,*]

[a] Department of Electronics Engineering, Kaunas University of Technology, Studentu St. 50, 51368 Kaunas, Lithuania
[b] Department of Mechatronics and Electronics, Faculty of Electrical Engineering and Information Technologies, University of Zilina 010 26 Zilina, Slovakia
[c] Faculty of Electrical Engineering and Communication, Brno University of Technology, 616 00 Brno, Czech Republic

ARTICLE INFO

Keywords:
Magnetic field sensors
AMR
Temperature drift
Temperature stability
Compensation

ABSTRACT

Magnetic field sensors are widely used in smart electronic systems for transportation, structural health monitoring, current sensing, geomagnetic navigation, and other applications. Among various sensor types, anisotropic magnetoresistance (AMR) sensors are often selected for their compact size, high sensitivity, and low cost. However, their performance is significantly affected by temperature-induced drift in magnetic field measurements. This study evaluates the temperature stability of three AMR sensors – LSM303AGR, LIS3MDL, QMC5883L – and a fluxgate sensor, DRV425. Results show that LSM303AGR demonstrates the best temperature stability in magnetic fields under 100 μT, with an average drift of 24.8 nT/K, and a sensitivity drift of −488 ppm/K, while LIS3MDL is suitable for measuring stronger fields due to its linear temperature characteristic despite a higher drift of 152.9 nT/K. Sensor measurement drift amounts to 12 % to 76 % of magnetic field threshold over a 50 °C range in practical reference application (10 μT), but algorithmic compensation using application-specific or diverse datasets can reduce drift to as low as 4.9–7.9 % of the reference threshold in fields under 100 μT. These findings highlight the importance of tailored compensation strategies when using AMR sensors for reliable long-term magnetic field monitoring.

1. Introduction

Nowadays smart electronic systems rely heavily on magnetic field measurement techniques to ensure their proper functionality. In smart transportation systems magnetic field change across traffic lanes provides means to identify vehicles, calculate their speed and estimate traffic [1–4]. By measuring magnetic field deviations across materials, it is possible to evaluate their structural integrity, find defects [5–8]. Magnetic field measurement above a conductor is an alternative way to assess current flowing through it [6,9]. Evaluating magnetic field vectors direction is basis of geomagnetic navigation used in electronic compasses, control units for satellites, unmanned aerial or underwater vehicles [10,11].

Measurement of magnetic field can be performed using various types of magnetic sensors. In this paper properties and characteristics of anisotropic magnetoresistance sensors (AMR) will be analyzed. Their major advantages are the ease of manufacture, high sensitivity, and compact footprint, which makes them low-cost and convenient [12–14].

However, their measurements suffer from temperature stability issues – the readings drift as the temperature changes. This is a critical and often limiting design factor for systems that need to measure the change of magnetic field induction over an extended period. For example, the practical importance of reliable sensor networks has been demonstrated in critical applications such as cognitive radio-based medical sensor networks for field hospitals [15] and long-term data collection and analysis applications such as networks for smart agriculture [16]. Moreover, magnetic field sensors can be used in communication systems, for example, as receivers for low-frequency rotating permanent

* Corresponding author.
E-mail addresses: matas.tamulynas@ktu.lt (M. Tamulynas), eidenis.kasperavicius@ktu.lt (E. Kasperavičius), vytautas.markevicius@ktu.lt (V. Markevičius), dangirutis.navikas@ktu.lt (D. Navikas), mindaugas.zilys@ktu.lt (M. Žilys), algimantas.valinevicius@ktu.lt (A. Valinevičius), michal.frivaldsky@fel.uniza.sk (M. Frivaldsky), sotner@vut.cz (R. Sotner), jan.jerabek@vut.cz (J. Jerabek), darius.andriukaitis@ktu.lt (D. Andriukaitis).

https://doi.org/10.1016/j.aeue.2025.156082
Received 10 September 2025; Accepted 11 October 2025
Available online 13 October 2025

magnet antennas, allowing low-latency and low-attenuation directional communication through concrete walls in pipeline monitoring systems [17].

In literature, the effect of temperature drift on magnetic field sensor measurements is considered to be linear [18]. It is described using two terms – offset drift and sensitivity change [19].

Offset drift with coefficient k_o (Fig. 1, right) is observed when no external magnetic field is present (measurement is non-trivial as it requires a Helmholtz coil) [20]. It affects the readings of the sensor by a fixed amount, which is only dependent on the temperature:

$$B' = B_0 + k_o \Delta T \tag{1}$$

where B' is the measured magnetic field, B_0 is the initial magnetic field, ΔT is the temperature change. Offset drift is measured in nT/K and has a magnitude of, for example, 100 nT/K [21].

Sensitivity change, described by coefficient k_s, depends on both the temperature and the external magnetic field [20]:

$$B' = B_0 + k_s B_0 \Delta T \tag{2}$$

It is measured by subtracting the associated offset drift from the sensor temperature characteristic. In general, as the magnetic field increases away from 0 T, the temperature drift associated with the sensitivity change increases in the opposite direction.

Sensitivity change is measured in ppm and has a magnitude of, for example, 600 ppm/K [21].

The aggregate effect of temperature on the measurement can be expressed as

$$B' = B_0 + k_o \Delta T + k_s B_0 \Delta T = B_0 + k \Delta T \tag{3}$$

where k is the aggregate temperature coefficient measured in practical applications

$$k = k_o + B_0 k_s \tag{4}$$

The temperature effect is large, often underestimated by manufacturers [20], and should be considered in practical applications. Fig. 2 shows an example of a LIS3MDL magnetometer used in a parking sensor application. In this instance, the magnetic field drift for the z-axis is around 45 μT with a temperature change of around 40 °C. This is significant in comparison to the vehicle detection threshold of 10 μT.

2. Related works

Most existing literature on the temperature stability of magnetic field sensors analyzes a single type of sensor. In [23] the difference between magnetic field sensors from the same batch were analyzed. Measured drift for the HMC1022 sensor was 20 μT over 76 °C.

[24] measured a temperature drift of 200 nT over 30 °C for the HMC1001 sensor. They also theorized that the difference between sensor temperature characteristics is caused by material temperature dependence, which differs from sample to sample.

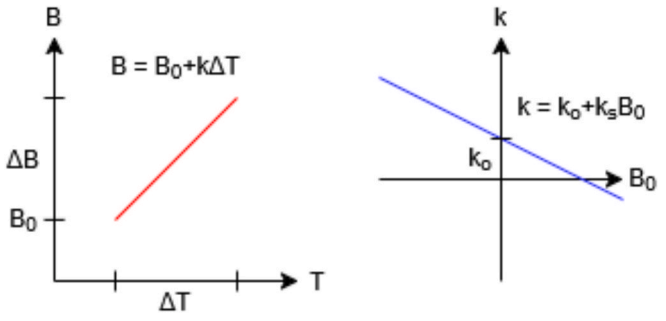

Fig. 1. Temperature effect mechanisms [22].

Papers on developing novel types of sensors also provide useful information. [25] developed a new AMR sensor and measured its characteristics – the uncompensated temperature coefficient of sensitivity 0.25 %/K and the offset drift 10 nT/K.

In a description by Honeywell [26], the sensitivity coefficient of the HMC1201 sensor was measured at −2500 ppm/°C.

Other research focuses on measuring temperature stability for sensors in existing applications. [27] determined that fluxgate sensors used in observatory equipment (Narod triaxial ring-core, DMI FGE, LEMI-17, and DIDD system) have a maximal residual of 2 nT over 50 °C temperature range. [28] measured 4 nT offset drift and 35 % sensitivity change over 400 °C for a bespoke magnetometer on a spacecraft.

[29] measured the effect of temperature on a compass – 0.1 ° over 1 °C. [30] determined that the sensor SFG-0.3 drifts by more than 1.5 % of scale over the range of 80 °C.

Popularity of magnetic sensors rose in 1990 and since then more than 50 % of all patents using magnetic sensors were based on magnetoresistance principle. However, publications such as [31], which evaluate and improve the properties of giant or tunnelling magnetoresistance (GMR and TMR) sensors (this paper improves the linearity of the Wheatstone bridge using an on-chip circuit) are significantly more common, compared with AMR sensors. This shows a clear gap in scientific literature [32].

Temperature drift represents a significant source of measurement error in AMR sensors. Yet, this effect is frequently understated in manufacturer datasheets [20], and comparative analyses of temperature stability are lacking in academic works. Therefore, this paper aims to compare sensitivity and offset drift of three AMR sensors and one fluxgate sensor with optional algorithmic compensation methods. The resulting benchmark is intended to aid the development of systems requiring long-term magnetic field monitoring.

This paper expands on the work in Tamulynas et al. [22] where the temperature drift characteristics of LSM303AGR sensors were analyzed.

3. Experimental setup

Four sensor models are analyzed: LIS3MDL [33] and LSM303AGR [34] by STMicroelectronics, QMC5883L [35] by QST, and a fluxgate sensor DRV425 [36] by Texas Instruments. Their parameters are summarized in Table 1.

LIS3MDL sensors have the highest sensitivity – their minimum field range is configurable to 400 μT. On the other hand, they have the highest value of noise and no internal temperature compensation algorithm. LSM303AGR sensors have the lowest sensitivity and highest measurable field range with configurable internal temperature compensation. QMC5883L sensors are an intermediate choice – they offer high sensitivity, average magnetic field range, and temperature drift compensation at the lowest price.

DRV425 fluxgate sensors have the lowest readings noise, best temperature stability parameters (sensitivity and offset drift), and the smallest hysteresis. Its measurable field range is up to 2 mT but it is also the most expensive sensor of all four. All sensors operate in a similar temperature range from −40 °C to 85 °C with the DRV425 being capable of functioning at 150 °C.

Equipment used for data acquisition includes a 90 x 100 mm PCB with 5 evenly spaced groups of 4 types of sensors for a total of 20 magnetic sensors (Fig. 3, a). SNOL 24/200 electric oven was used to create and control the environment temperature. Magnetic sensor readings were collected using an STM32 microcontroller and transmitted via Wi-Fi (Fig. 3, b).

All measurement cycles started with the PCB being placed in the oven and heated to 65 °C. After the temperature was reached, the oven was turned off, and the sensor data was collected at 100 Hz as the sensors and the PCB cooled down to 27 °C.

17 experiments were performed and analysed – 10 experiments in magnetic field up to 100 μT and 7 experiments in magnetic fields 100 μT

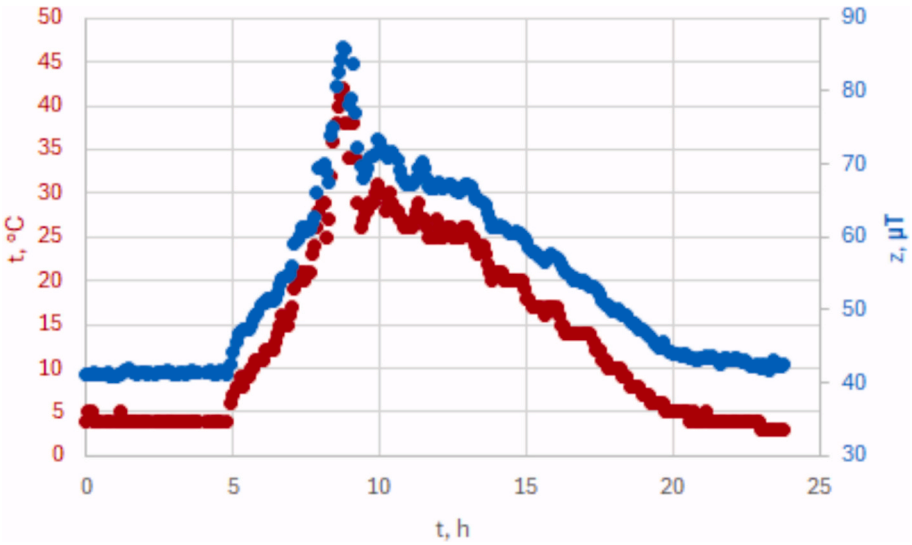

Fig. 2. The effect of temperature on an AMR sensor used in a parking sensor application.

Table 1
Summary of magnetic field sensor parameters.

Parameter		Sensor			
		LIS3MDL	LSM303AGR	QMC5883L	DRV425
Magnetic field range, μT	Max	±1600	±4915.2	±800	±2000
	Min	±400		±200	
Sensitivity, nT/LSB	Max	14.62@ ±400 μT	139.5	8.33@ ±200 μT	55.03 (R_{Shunt} = 300 Ω)
	Min	58.45@ ±1600 μT	160.5	33.33@ ±800 μT	750.43 (R_{Shunt} = 22 Ω)
Sensitivity drift, %/°C		–	±0.03	–	±7 ppm FS
Linearity, %FS		±0.12	–	0.1@±200 μT	±0.1
Hysteresis		–	–	0.3 %FS	1.4 μT @ −10 mT to 10 mT
Offset, μT		±100	±6	±1	±10
Offset drift, nT/°C		–	±30	–	±5
Operating temperature, °C	Max	85	85	85	150
	Min	−40	−40	−40	−50
Magnetic readings noise, μT	Max	1.16 (Z axis)	0.849	–	0.048 + 0.433 (from ADC)
	Min	0.905 (X and Y axis)			0.048 + 0.032 (from ADC)
Internal temperature compensation		–	Configurable	Fixed	–
Price, €		2.14	2.9	0.91	4.64

to 819 μT. In this paper, weaker than 100 μT external fields are referred to as "normal", ones exceeding this value – "strong".

Magnetic field readings of the *x*, *y*, and *z* axes were collected for LSM303AGR, LIS3MDL, QMC5883L sensors, and of the *z* axis for DRV425 sensors. During the experiments, the magnetic field range of LIS3MDL sensors was set to ±400 μT, LSM303AGR ± 4915.2 μT, QMC5883L ± 800 μT. The range of DRV425 was set to ±100 μT in "normal" magnetic fields and ±1000 μT in "strong" magnetic fields.

4. Results

LIS3MDL sensor in the temperature range from 30 °C to 65 °C shows consistently linear magnetic drift characteristic (Fig. 4). As the temperature increases, so does the *absolute value* of the measured magnetic field. The average noise measured was 0.75 μT.

The plot of the temperature coefficient k against the external magnetic field B_0 displays a consistent linear dependence (Fig. 5). The aggregate temperature coefficient follows a downward trend as the value of the external magnetic field increases.

The average LIS3MDL sensor has an offset coefficient $k_o = 13.9$ nT/K and sensitivity coefficient $k_s = -803$ ppm/K based on the linear trendline fitted to this data. A statistical summary of measured coefficient values is presented at the end of the paper, in Table 2.

The offset and sensitivity of individual sensor axes have smaller confidence intervals (CIs) compared to the sensors overall. However, their size is not consistent (Fig. 6 shows one of the sensors with the smallest individual axis CIs).

In any case, the coefficients differ between sensors of different or even same type, and between axes of the same sensor. Near 0 T for any specific axis (without external field), this distribution results in a change of sign of k. Depending on the measurement, the coefficient can be positive or negative. This behavior is observed for all types of sensors analyzed in this paper.

Data from multiple measurements (Fig. 5) demonstrates that a general trend exists regardless of differences between axes. It can be approximated as a linear model with a 95 % CI of ±330 nT/K.

In addition to the static temperature effect, a dynamic characteristic (hysteresis) takes effect (Fig. 7). Most likely, its existence is caused by nearby components (e.g., surface mount resistors or capacitors on a PCB) inducing an additional magnetic field in the sensor due to their internal magnetization as in Markevicius and Navikas [23]. In this figure, the first thermal cycle has a significant difference between readings of the heating and cooling cycles. Such an effect is no longer noticeable in subsequent temperature cycles.

In practice, the effects of hysteresis can be avoided by using demagnetization equipment or performing a thermal cycle – before deploying each unit or periodically in case there is a risk of magnetization in application.

LSM303AGR sensor, similarly to LIS3MDL, has a linear temperature characteristic (Fig. 8). However, the LSM303AGR features an internal temperature compensation mechanism that significantly improves temperature stability. When compensation is turned on, as a side effect,

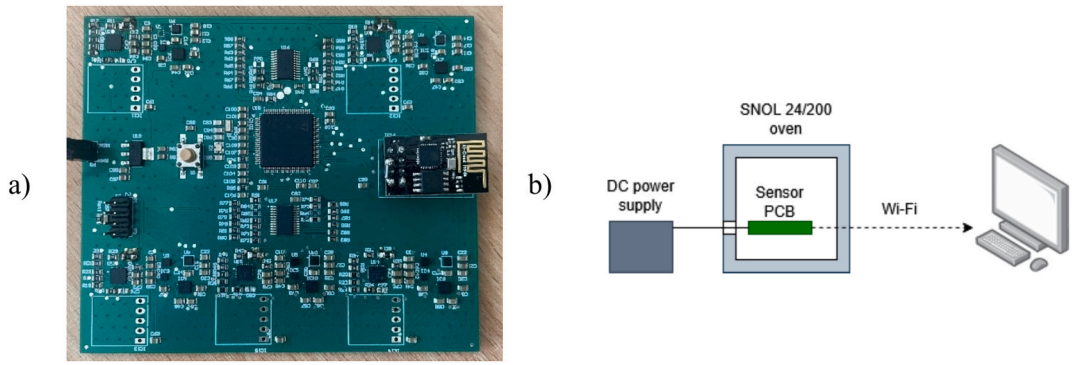

Fig. 3. Sensor printed circuit board (a) and the experiment setup (b).

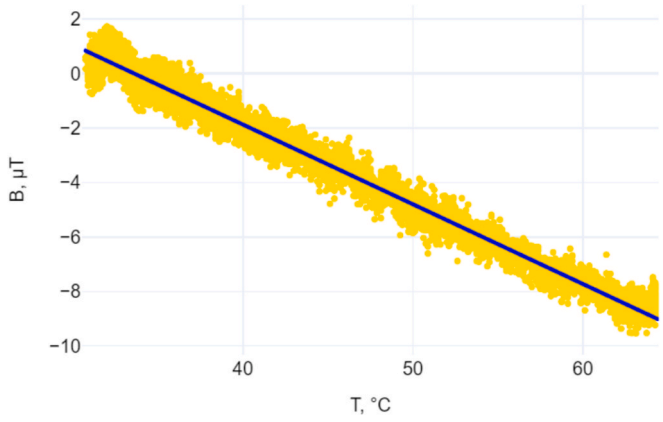

Fig. 4. Temperature drift of LIS3MDL readings and its linear trendline.

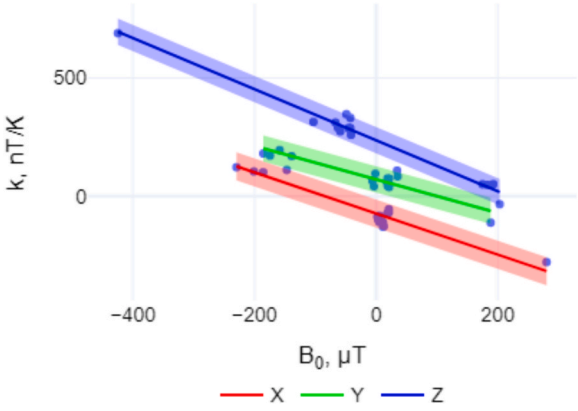

Fig. 6. *x*, *y*, and *z*-axis temperature characteristics of one LIS3MDL sensor.

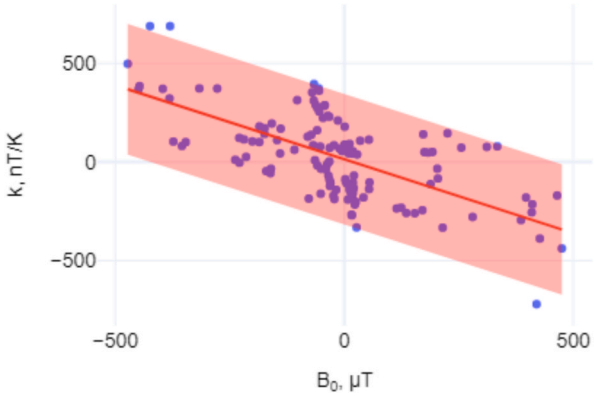

Fig. 5. Temperature coefficient dependence on external magnetic field with a 95 % confidence interval (shaded area) of LIS3MDL sensor.

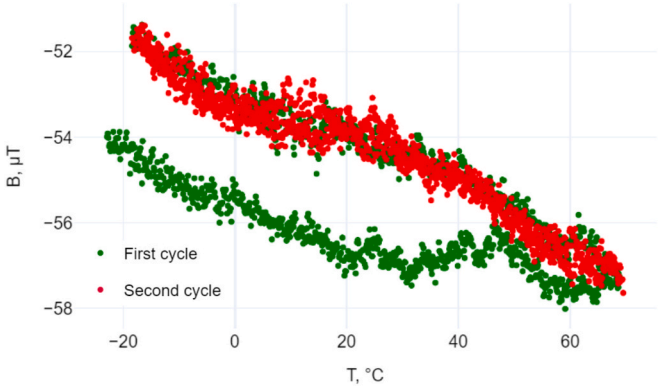

Fig. 7. Data from the first and second thermal cycles of the LIS3MDL sensor visualising thermal hysteresis.

Table 2
Temperature coefficient values for all sensors in "normal" fields.

Sensor		LIS3MDL	LSM303AGR	QMC5883L	DRV425
k, nT/K	Maximum	570.1	84.6	149.3	91.4
	Average	152.9	24.8	46.3	20.8
	Minimum	3.14	0.44	0.48	0.07
Measurement drift	Maximum	28.51	4.23	7.46	4.57
ΔT = 50 K, μT	Average	7.65	1.24	2.31	1.04
	Minimum	0.16	0.022	0.024	0.004
k_o, nT/K		13.9	1.3	7.6	1.8
k_s, ppm/K		−803	−488	−2231	−512
95 % CI, nT/K		±330,6	±91,9	±122,4	±60,8

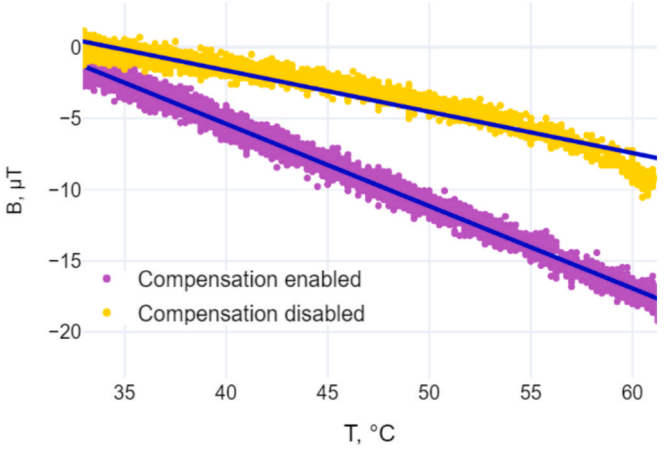

Fig. 8. Effect of non-linear internal temperature compensation of LSM303AGR sensor.

it makes the characteristic non-linear in temperatures higher than 55 °C or in "strong" fields. The non-linear characteristic can be approximated using a second-order polynomial trendline. Measurement noise, regardless of sensor configuration, is around ±0.5 μT.

The coefficient dependence on the external magnetic field is also linear (Fig. 9), though sensitivity k_s of the LSM303AGR is smaller than that of the LIS3MDL (former has better temperature stability in "strong" fields).

On average, LSM303AGR sensors have an offset coefficient $k_o = 1.3$ nT/K and sensitivity coefficient $k_s = -488$ ppm/K. The 95 % confidence interval for the linear model is ±92 nT/K.

QMC5883L sensor, similarly to the LSM303AGR sensor, has a temperature compensation function. However, its behavior is discrete rather than continuous – there are distinct jumps in the temperature characteristic as shown in Fig. 10.

From the magnetic drift characteristic, significant periodic jumps can be observed at a temperature change of 10.24 °C or 1024 LSB, given a temperature sensitivity of 0.01°C/LSB. The jumps happen instantaneously at a single magnetic value reading and occur for all axes simultaneously. The exact temperature of the jump is different across sensors but is constant for a specific sensor even after multiple power off–on cycles. The height of the jump increases with the magnitude of the external magnetic field. Therefore, they are most noticeable during experiments with "strong" fields.

For all sensors, one jump is missing in the region of 10 °C to 23 °C (Fig. 11), which results in rotational symmetry based on the missing jump point. If T_{ref} is the symmetry point (reference temperature), then the n-th jump location is

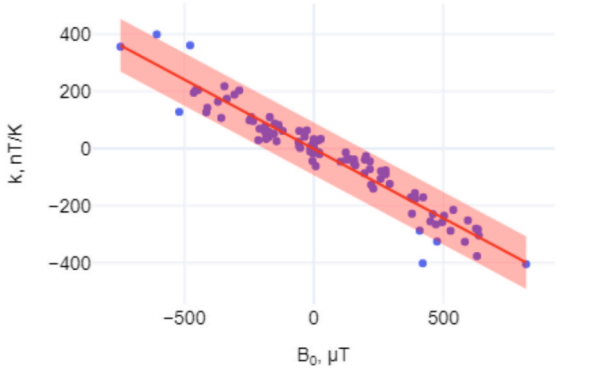

Fig. 9. LSM303AGR temperature coefficient dependence on external magnetic field.

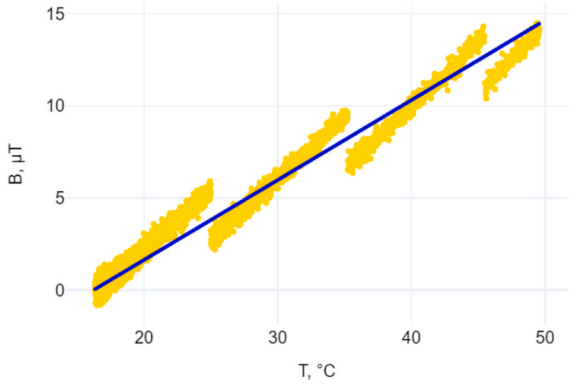

Fig. 10. Temperature characteristic of QMC5883L sensor.

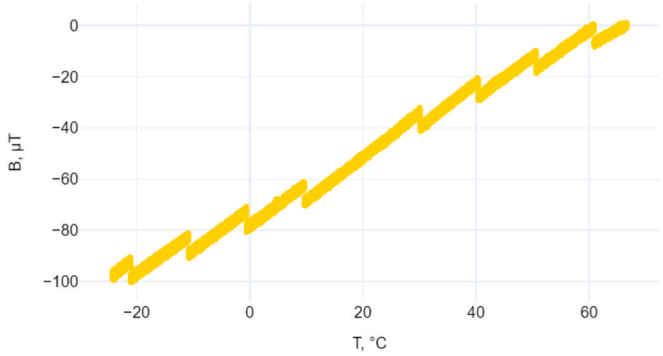

Fig. 11. Non-existent jump at the temperature value of 19.89 °C for the QMC5883L sensor.

$$T_n = T_{ref} + 10.24n, n \in \mathbb{Z}\backslash\{0\} \quad (5)$$

Overall, the QMC5883L coefficient dependence on external magnetic field is linear but large in magnitude (Fig. 12).

Its offset drift coefficient is $k_o = 7.6$ nT/K, sensitivity coefficient is $k_s = -2231$ ppm/K. The 95 % confidence interval for the linear model is ±122 nT/K. Measurement noise is around ±0.75 μT.

DRV425 fluxgate sensor was selected for comparison with the AMR sensors. Its temperature characteristic is linear (Fig. 13), although less data is available due to the sensor measuring only z-axis instead of three axes.

The measurement noise for this sensor is around ±0.35 μT, offset drift coefficient $k_o = 1.8$ nT/K, sensitivity coefficient $k_s = -512$ ppm/K. The 95 % confidence interval for the linear model is ±60 nT/K.

A summary of uncompensated sensor temperature coefficients

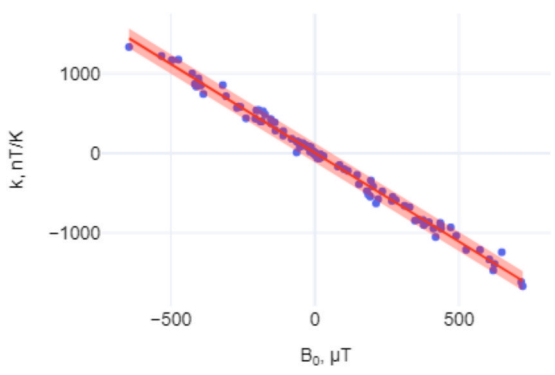

Fig. 12. Temperature coefficient dependence on external magnetic field of QMC5883L sensor.

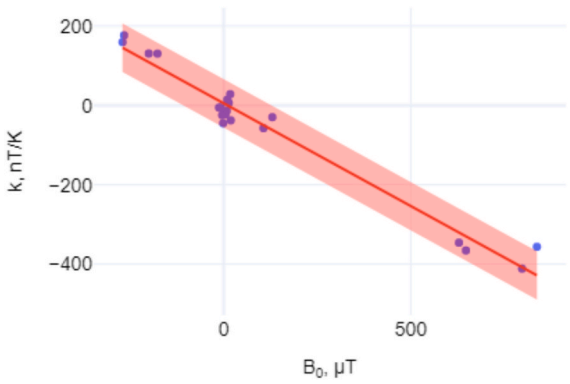

Fig. 13. Temperature coefficient dependence on external magnetic field of DRV425 sensor.

is given in Table 2. Average coefficient k is presented for measurements in "normal" fields, for which the differences in k are mostly caused by sensor differences and not differences in B_0. In addition, expected measurement drift over $\Delta T = 50$ K is given for reference in system design.

Each type of sensor has a wide distribution of coefficient values. Some tested units had excellent temperature stability down to 0.1 nT/K while others had more than 1300 times worse coefficients (see DRV425 minimum and maximum values). The CI of the linear sensor model was smallest for the sensors with the lowest k_s (DRV425, LSM303AGR) and largest for LIS3MDL – 3.5 times larger than that of the LSM303AGR. The CIs are visualized in Fig. 14.

In "normal" fields, the fluxgate sensor DRV425 was the most stable, followed by LSM303AGR. LIS3MDL performed the worst, over 7 times worse than DRV425. Similar characteristics were observed with maximum coefficient values. All AMR sensors had similar noise amplitudes at about two times larger than that of the DRV425.

The coefficient of sensitivity k_s was the smallest for LSM303AGR – with compensation enabled, it outperformed the fluxgate DRV425. Largest k_s was measured for QMC5883L, which makes the measurement drift extreme at "strong" fields.

As seen in real-world applications, the temperature of AMR sensors can change by 40 °C over just a few hours. Since the typical vehicle detection threshold is 10 μT, the measured drift over 50 °C from Table 2 is significant: 76 % of threshold value for LIS3MDL, 12 % for LSM303AGR, 23 % for QMC5883L and 10 % for DRV425.

5. Measurement drift compensation

Measurement drift of AMR sensors can be reduced by obtaining an estimate of temperature coefficients $\hat{k}_s$ and $\hat{k}_o$ (or aggregate coefficient $\hat{k}$) and applying them to sensor readings to get the estimated field value

$$\widehat{B} = B' - \widehat{k}\Delta T, \tag{6}$$

where B' is the measured magnetic field, ΔT is the temperature change.

This paper analyzes 3 compensation methods which were derived from the methods described in [22]:

- *Single-measurement compensation method* – given one individual sensor, one measurement (*experimental procedure described in chapter 3*) of $\hat{k}$ is performed and the coefficients $\hat{k}_x$, $\hat{k}_y$, $\hat{k}_z$ are obtained; these coefficients are applied to each axis of this individual sensor for any subsequent measurements.
- *Multi-measurement compensation method* – instead of one measurement, 3 or more measurements are completed for one individual sensor; $\hat{k}_s$ and $\hat{k}_o$ are calculated for each axis from the linear trendline of the gathered points; for each axis of any subsequent measurements, the coefficient $\hat{k}$ is calculated and applied according to (6).
- *Multi-sensor compensation method* – instead of one individual sensor, 3 or more sensors are selected; combined $\hat{k}_s$ and $\hat{k}_o$ are calculated for all axes; from there, the procedure is the same as for the multi-measurement method.

These methods differ both in the difficulty of application and expected results. Multi-sensor compensation is most cost-effective since measurements done on a test batch of sensors can be applied to sensors in mass production. Multi-measurement compensation is only viable for small samples because each sensor must be measured individually. However, the methods consisting of several measurements offer better statistical precision than single-shot compensation.

The effect of compensation methods is compared by calculating the residual temperature coefficient

$$k_r = k - \widehat{k}, \tag{7}$$

where k is the aggregate temperature coefficient measured in practical applications, $\hat{k}$ – estimating temperature coefficient derived with compensation methods.

The *single-measurement method* improved the temperature stability in tests where the application magnetic field was similar ("strong" or "normal") to the measurement field. In "normal" fields, it reduced the temperature coefficient by 11 % (LSM303AGR) to 81 % (LIS3MDL) while in "strong" fields it reduced the coefficient by 33 % (QMC5883L) to 88 % (DRV425).

Since this method assumes the sensitivity to be zero, the offset can only be compensated for measurements in similar fields (e.g., "normal" fields or permanent magnet in a fixed position). Single-measurement compensation in weak fields does not apply to DRV425 because its coefficient CI is larger than the temperature coefficient k. Results for different sensors are visualized in (Fig. 15 and Fig. 16).

The *multi-measurement method* consistently outperformed the single-measurement method because it reduces the impact of outlier measurements. If measurement dataset was collected in similar or diverse fields (*either the same strength magnetic field as in-application or combination of both "normal" and "strong" fields*), it reduced the measurement drift in "normal" fields by 10 % (DRV425) to 88 % (LIS3MDL) and in "strong" fields by 81 % (LSM303AGR) to 98 % (QMC5883L).

Measurements in "strong" fields cannot be used to compensate measurements in weak fields due to large measurement confidence intervals, except for LIS3MDL – the coefficient CI itself is large enough compared to measurement CI. Additionally, there was not enough data for DRV425 to perform both measurement and application in "strong" fields.

The *multi-sensor method* is only applicable to applications in "strong" fields where the differences between sensors are small compared to the measured field. In "normal" fields, it only improved temperature

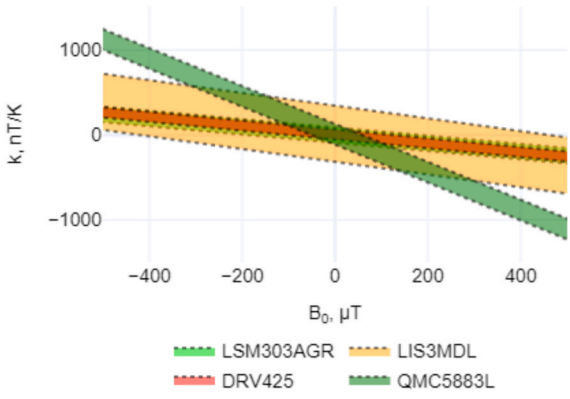

Fig. 14. 95 % confidence intervals of the temperature coefficient linear models.

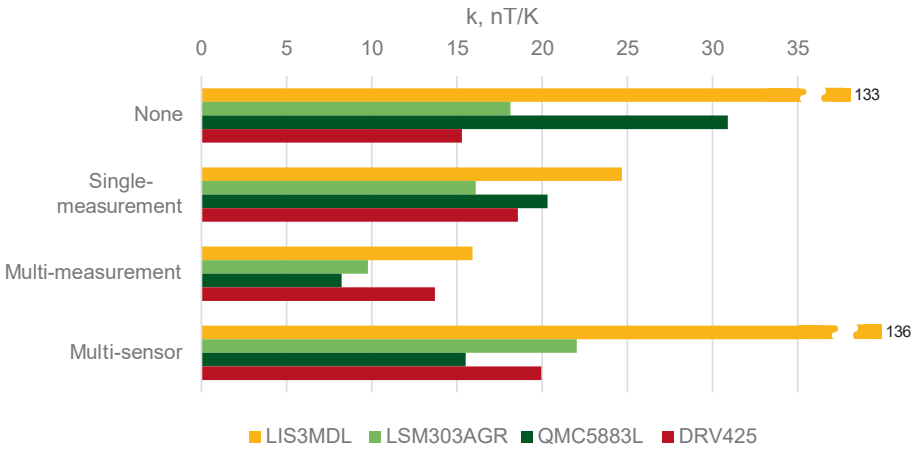

Fig. 15. Residual temperature coefficient after compensation when the measurement and application fields are under 100 μT.

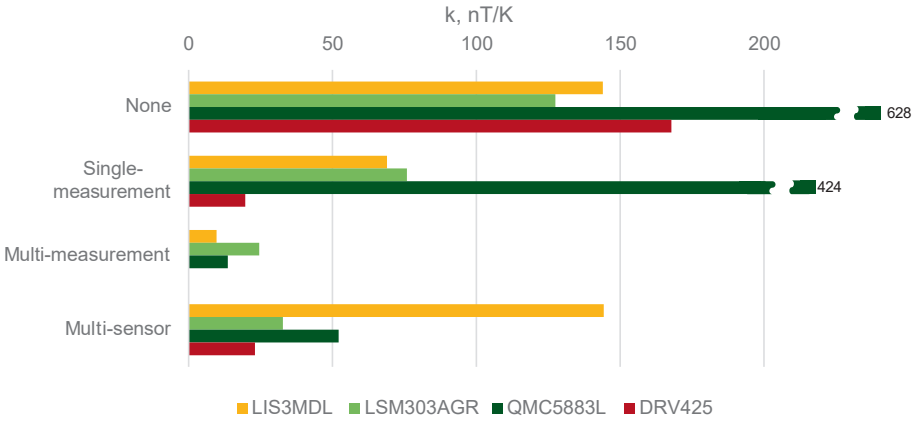

Fig. 16. Residual temperature coefficient after compensation when the measurement and application fields over 100 μT.

stability for QMC5883L (50 %) because of its large k_s. In "strong" fields, this method improved stability for LSM303AGR (74 %), QMC8553L (92 %), and DRV425 (86 %) but not LIS3MDL because of its large CI.

These results show that while compensation for the measurement drift is possible, its effect is different for the two types of measured external field ("normal" or "strong"). For the calculation of $\hat{k_s}$ and $\hat{k_o}$ the measurement dataset must be similar to application conditions ("normal" or "strong" field) or have a diverse range of field values. This is necessary because measurements in "normal" fields depend mainly on $\hat{k_o}$ and lead to inaccurate $\hat{k_s}$ estimates, while measurements in "strong" fields depend mainly on $\hat{k_s}$ and lead to inaccurate $\hat{k_o}$ estimates.

Overall, single-measurement and multi-measurement methods can be applied in "normal" fields, which results in QMC5883L being the most stable sensor (median $k = 8.2$ nT/K), followed by LSM303AGR with multi-measurement compensation method. Though single-measurement and multi-measurement methods improved the stability of LIS3MDL, it is still the least stable sensor.

The multi-measurement method is not recommended – it is much more labor-intensive but yields only up to 2 times better temperature stability. The multi-sensor method does not improve stability due to offset drift differences between sensors.

In "strong" fields, multi-measurement and multi-sensor methods are applicable. Using the multi-measurement method reduces drift up to 98 % – the most stable sensor is LIS3MDL, followed by QMC5883L.

Multi-sensor method is labor-efficient but less effective. In "strong" fields it is applicable for all sensors except LIS3MDL which has a large coefficient CI. This method improves stability up to 92 %, with the best results achieved with the LSM303AGR sensor.

In practical applications, compensation reduces temperature drift in "normal" fields to below 10 % of vehicle detection threshold. Multi-measurement method results in 7.9 % drift for LIS3MDL, 4.9 % for LSM303AGR, 8.2 % for QMC5883L, 6.8 % for DRV425. Single-measurement method results are approximately two times worse.

6. Conclusions

Temperature-induced magnetic measurement drift of anisotropic magnetoresistance sensors LSM303AGR, LIS3MDL, QMC5883L, and fluxgate sensor DRV425 were evaluated. The LIS3MDL and DRV425 measurements have linear temperature characteristics, while LSM303AGR has a non-linear characteristic above 55 °C or in magnetic fields above 100 μT, QMC5883L has a sawtooth characteristic due to internal compensation. Of the tested AMR sensors, LSM303AGR has the best average temperature stability at 24.8 nT/K in magnetic fields below 100 μT and sensitivity drift of −488 ppm/K. LIS3MDL sensor has the worst average temperature stability at 152.9 nT/K but it can be used in stronger magnetic fields as it has a linear temperature characteristic.

AMR sensors should not be used for long-term magnetic field measurement without algorithmic compensation because their drift over the range of 50 °C amounts to 12 % to 76 % of reference vehicle detection threshold (10 μT). Compensation methods with a specifically selected dataset (tailored to application magnetic field or diverse) can improve temperature stability. Single-measurement and multi-measurement methods can be used for applications in magnetic fields below 100 μT, leading to reduced drift of 4.9 % to 7.9 % of reference threshold. Multi-measurement and multi-sensor methods can be used in stronger

magnetic fields.

Future work based on this research could focus on verifying the applicability of temperature compensation methods. Most importantly, it could include experiments in different magnetic field sensor applications and analysis of the initial and compensated temperature related errors.

CRediT authorship contribution statement

Matas Tamulynas: Writing – review & editing, Writing – original draft, Visualization, Software, Investigation, Conceptualization. **Eidenis Kasperavičius:** Writing – review & editing, Writing – original draft, Visualization, Software, Investigation, Data curation. **Vytautas Markevičius:** Validation, Methodology, Conceptualization. **Dangirutis Navikas:** Validation, Supervision, Methodology, Data curation. **Mindaugas Žilys:** Resources, Funding acquisition, Formal analysis. **Algimantas Valinevičius:** Validation, Funding acquisition, Formal analysis. **Michal Frivaldsky:** Software, Resources. **Roman Sotner:** Writing – review & editing, Resources, Investigation, Data curation. **Jan Jerabek:** Writing – review & editing, Investigation, Formal analysis, Data curation. **Darius Andriukaitis:** Writing – original draft, Supervision, Project administration, Investigation, Funding acquisition.

Declaration of competing interest

The authors declare the following financial interests/personal relationships which may be considered as potential competing interests: Darius Andriukaits reports financial support was provided by Research Council of Lithuania (LMTLT), agreement no. S-A-UEI-23-1 (22 December 2023). N/A If there are other authors, they declare that they have no known competing financial interests or personal relationships that could have appeared to influence the work reported in this paper.

Acknowledgements

This research has received funding from the Research Council of Lithuania (LMTLT), agreement no. S-A-UEI-23-1 (22 December 2023).

Data availability

No data was used for the research described in the article.

References

[1] Miklusis D, Markevicius V, Navikas D, Ambraziunas M, Cepenas M, Valinevicius A, et al. Erroneous vehicle velocity estimation correction using anisotropic magnetoresistive (AMR) sensors. Sensors 2022;22:8269. https://doi.org/10.3390/s22218269.

[2] Soni N, Malekian R, Andriukaitis D, Navikas D. Internet of vehicles based approach for road safety applications using sensor technologies. Wirel Pers Commun 2019;105:1257–84. https://doi.org/10.1007/s11277-019-06144-0.

[3] Wang K, Xiong H, Zhang J, Chen H, Dou D, Xu C-Z. SenseMag: enabling low-cost traffic monitoring using noninvasive magnetic sensing. IEEE Internet Things J 2021;8:16666–79. https://doi.org/10.1109/JIOT.2021.3074907.

[4] Balamutas J, Navikas D, Markevičius V, Čepėnas M, Valinevičius A, Žilys M, et al. Passing vehicle road occupancy detection using the magnetic sensor array. IEEE Access 2023;11:50984–93. https://doi.org/10.1109/ACCESS.2023.3278986.

[5] Yalçın S. Fault detection in steel belts of tires using magnetic sensors and different deep learning models. FUJECE 2025;4:85–99. https://doi.org/10.62520/fujece.1527246.

[6] Nicolicea A, Oliveros-Mata ES, Makarov D, Melzer M, Pelkner M. Flexible anisotropic magnetoresistive sensors for novel eddy current testing applications. Measurement 2025;253:117340. https://doi.org/10.1016/j.measurement.2025.117340.

[7] Eslamlou AD, Ghaderiaram A, Schlangen E, Fotouhi M. A review on non-destructive evaluation of construction materials and structures using magnetic sensors. Constr Build Mater 2023;397:132460. https://doi.org/10.1016/j.conbuildmat.2023.132460.

[8] Stamou G, Angelopoulos S, Ktena A, Hristoforou E. 3D Anisotropic Magnetoresistance sensor for steel health monitoring. Eng Fail Anal 2024;160:108165. https://doi.org/10.1016/j.engfailanal.2024.108165.

[9] Shi Z-Y, Gao W, Wang Q, Guo H, Tang J, Li Z-H, et al. Current sensor based on diamond nitrogen-vacancy color center. Chin Phys B 2023;32:070704. https://doi.org/10.1088/1674-1056/acc3fe.

[10] Zhao H, Zhang N, Xu L, Lin P, Liu Y, Li X. Summary of research on geomagnetic navigation technology. IOP Conf Ser: Earth Environ Sci 2021;769:032031. https://doi.org/10.1088/1755-1315/769/3/032031.

[11] Zhang S, Cui M, Zhang P. Development and application of a high-precision portable digital compass system for improving combined navigation performance. Sensors 2024;24:2547. https://doi.org/10.3390/s24082547.

[12] Khan MA, Sun J, Li B, Przybysz A, Kosel J. Magnetic sensors-a review and recent technologies. Eng Res Express 2021;3:022005. https://doi.org/10.1088/2631-8695/ac0838.

[13] Yang Z, Jiang Y. Prospective review of magneto-resistive current sensors with high sensitivity and wide temperature range. J Low Power Electron Appl 2024;14:43. https://doi.org/10.3390/jlpea14030043.

[14] Ritzinger P, Výborný K. Anisotropic magnetoresistance: materials, models and applications. R Soc Open Sci 2023;10:230564. https://doi.org/10.1098/rsos.230564.

[15] Timucin T, Bayrakdar S, Timucin EK, Bayrakdar ME. Enhancing cognitive radio sensor network security with smart contract for field hospitals. IEEE Sens J 2025:1. https://doi.org/10.1109/JSEN.2025.3598065.

[16] Demirtürk B, Enes BM. Cognitive sensor network-based emergency notification in smart agriculture. IEEE Sens J 2025;25:3631–9. https://doi.org/10.1109/JSEN.2024.3505267.

[17] Zhang Y, Cui Y, Wang C, Song X, Pei Y, Yuan Z. Rotating permanent magnet antenna array for directional communication in pipeline monitoring system. AEU-Int J Electron C 2024;177:155210. https://doi.org/10.1016/j.aeue.2024.155210.

[18] Liang C, Zhou Y, Zhang D, She X, Huang T, Shu X. Research on the temperature characteristic of magnetic sensor in the magnetic drift compensation fiber-optic gyroscope. Optik 2018;172:91–6. https://doi.org/10.1016/j.ijleo.2018.07.015.

[19] Ripka P, Butta M, Platil A. Temperature stability of AMR sensors. Sens Lett 2013;11:74–7. https://doi.org/10.1166/sl.2013.2807.

[20] Ripka P, Závěta K. Chapter Three Magnetic Sensors: Principles and Applications. In: Buschow KHJ, editor. Handbook of Magnetic Materials, vol. 18, Elsevier; 2009, p. 347–420. DOI: 10.1016/S1567-2719(09)01803-4.

[21] Ripka P, Janosek M. Advances in magnetic field sensors. Sens J IEEE 2010;10:1108–16. https://doi.org/10.1109/JSEN.2010.2043429.

[22] Tamulynas M, Kasperavičius E, Navikas D. Temperature stability and compensation of magneto resistance sensors. In: TiFEC–2025: Tifec Student Scientific Conference. Kaunas: Kaunas University of Technology; 2025. p. 40–3.

[23] Markevicius V, Navikas D. Adaptive thermo-compensation of magneto-resistive sensor. Elektronika Ir Elektrotechnika 2011;114:43–6. https://doi.org/10.5755/j01.eee.114.8.694.

[24] Včelák J, Ripka P, Platil A, Kubík J, Kašpar P. Errors of AMR compass and methods of their compensation. Sens Actuators, A 2006;129:53–7. https://doi.org/10.1016/j.sna.2005.09.048.

[25] Ripka P, Vopálenský M, Platil A, Döscher M, Lenssen K-M-H, Hauser H. AMR magnetometer. J Magn Magn Mater 2003;254–255:639–41. https://doi.org/10.1016/S0304-8853(02)00927-7.

[26] Pant B, Withanawasam L, Bohlinger M, Larson M, Ohme B. High temperature anisotropic magnetoresistive (AMR) sensors. Additional Conf (Device Packaging, HiTEC, HiTEN, & CICMT) 2015;2015:236–43. https://doi.org/10.4071/HiTEN-Session7-Paper7_1.

[27] Csontos A, Hegymegi L, Heilig B. Temperature Tests on Modern Magnetometers, 2006.

[28] Nishio Y, Tohyama F, Onishi N. The sensor temperature characteristics of a fluxgate magnetometer by a wide-range temperature test for a Mercury exploration satellite. Meas Sci Technol 2007;18:2721–30. https://doi.org/10.1088/0957-0233/18/8/050.

[29] Pham V-T, Nguyen D-C, Tran Q-H, Chu T, Tran D-T. Thermal Stability of Magnetic Compass Sensor for High Accuracy Positioning Applications 2015.

[30] Liu S, Fan J, Li W, Long Z, Hu K, Jiang X, et al. Experimental research on temperature characteristics of magnetic sensitive sensors. Second International Conference on Energy, Power, and Electrical Technology (ICEPET 2023), vol. 12788, SPIE; 2023, p. 1123–9. DOI: 10.1117/12.3005307.

[31] Sen T, Maity A, Sen S. On-chip implementation of different analog linearization schemes for giant-magnetoresistance sensors with a comparative study. AEU-Int J Electron C 2021;139:153903. https://doi.org/10.1016/j.aeue.2021.153903.

[32] Zheng C, Zhu K, Cardoso De Freitas S, Chang J-Y, Davies JE, Eames P, et al. Magnetoresistive sensor development roadmap (non-recording applications). IEEE Trans Magn 2019;55:1–30. https://doi.org/10.1109/TMAG.2019.2896036.

[33] STMicroelectronics. LIS3MDL 2023. https://www.st.com/en/mems-and-sensors/lis3mdl.html (accessed June 12, 2025).

[34] STMicroelectronics. LSM303AGR 2022. https://www.st.com/en/mems-and-sensors/lsm303agr.html (accessed May 29, 2025).

[35] QST Corporation Limited. QMC5883L 2016. https://www.qstcorp.com/en_comp_prod/QMC5883L (accessed June 12, 2025).

[36] Texas Instruments. DRV425. Texas Instruments 2016. https://www.ti.com/product/DRV425 (accessed June 12, 2025).